# A New Zero Voltage Transition Non-Isolated Bidirectional DC-DC Converter

# Podila Purna Chandra Rao<sup>1</sup>, Radhakrishnan Anandhakumar<sup>1</sup>, LaShanmukha Rao<sup>2</sup>

<sup>1</sup>Department of Electrical Engineering, Faculty of Engineering and Technology, Annamalai University, Chidambaram, India

The primary objective of this study is to examine and develop novel Zero Voltage Transition (ZVT) non-isolated bidirectional DC-DC converters specifically designed for battery storage purposes in hybrid electric vehicles. The initial focus is on a bidirectional converter (BDC) that has been specifically engineered to possess a high voltage gain. Additionally, this converter is equipped with the capability of performing soft-switching operations on Insulated Gate Bipolar Transistors (IGBTs). To attain minimized switching losses and enhanced efficiency, the primary insulated-gate bipolar transistors (IGBTs) are operated under zero-current conditions during the commutation phase from turn-on to turn-off state. The zero-current turn-off operation is achieved through the utilization of a soft-switched cell, comprising of a resonant inductor, capacitor, and supplementary IGBTs. A novel converter is suggested, which incorporates zero-voltage transition operation for the insulated-gate bipolar transistors (IGBTs). The performance of the hard-switched bridgeless dc-dc converter (BDC) has been enhanced with the incorporation of supplementary soft-switched cells. The soft-switched cell is composed of resonant inductors, capacitors, and auxiliary switching devices. The softswitched cell has been utilized to achieve zero voltage turn-on of the primary insulated-gate bipolar transistors (IGBTs). The operation of this converter involves charging the battery in the buck mode and utilizing the charged battery to give the desired output voltage in boost mode. This study involved doing a design simulation analysis on a high-gain bidirectional converter (BDC) within a 70V/300V power system. The converter was evaluated under an operating frequency of 50kHz, with a maximum output power of 800W. The high-gain

<sup>&</sup>lt;sup>2</sup>Department of Electrical and Electronics Engineering, Kallam Haranadhareddy institute of technology, Dasaripalem, India

soft-switched BDC demonstrated an efficiency of 96.5% in boost mode and 97% in buck mode. This study presents the operational principles, design analysis, and simulation assessments.

**Keywords:** DC-DC converter, Solar PV system, MPPT, PWM, High gain, Zeta Converter.

#### 1. Introduction

The applications that include battery storage are benefiting significantly from the use of DC-DC converters. When building the topologies, the characteristics like efficiency and switching power losses are the variables that will improve the performance of these converters and offer the best option to pick an efficient converter for the industrial applications. These factors are also the aspects that will improve the performance of these converters. Research on soft-switched bidirectional converters is currently being conducted. with a particular emphasis on its use in battery storage applications (such as supercapacitors and fuel cells). In order to achieve a zero-voltage transition for a DC-DC boost converter, auxiliary resonant switches [1] have previously been the subject of research. The softswitched bidirectional converters [1-6] were developed using simple auxiliary circuits (coupled inductors, self-commutation, and an auxiliary cell). These soft-switched bidirectional converters are appropriate for battery chargers that are run under extremely low output power levels with greater efficiency. In a similar fashion, the research is concentrated not only on ZVT but also on the zero current switching operation of the switches. These switches were developed with the auxiliary resonant cells [7] for the battery storage applications and a high voltage gain zero voltage switching isolated DC-DC converter [8]. Additionally, the soft-switching was obtained with the assistance of leakage inductance and additional snubber capacitor with the main IGBTs. Within the context of the applications of energy storage systems in electric cars, this chapter presents a novel ZVT bidirectional DC-DC converter as a potential solution. Either the boost or the buck mode may be used with the suggested converter. In order to achieve a transition of zero voltage to the main switches, a novel non-isolated converter was suggested in this chapter. This converter would make use of resonant components and would work in conjunction with auxiliary active devices. The improved efficiency and decreased turn-on losses offered by this converter are the primary benefits it offers. This chapter provided an overview of ope The usage of DC-DC converters has shown to be of great use to applications, such as battery storage, which make use of the technology. During the process of creating the topologies, the features such as efficiency and switching power losses are the factors that will increase the performance of these converters and provide the best choice to pick an efficient converter for the applications that are used in industrial settings. These elements are also the components that will contribute to an improvement in the functionality of these converters. In recent decades, there has been a focus on research on soft-switched bidirectional converters, in particular for applications requiring battery storage (Super-cap, Fuel cell). This is because these converters are more flexible and easier to use. Auxiliary resonant switches [1] have already been the focus of study in an effort to realise a zero-voltage transition for a DC-DC boost converter. Simple auxiliary circuits (coupled inductors, self-commutation, and an auxiliary cell) were used in the development of soft-switched bidirectional converters [1-6]. These soft-switched bidirectional converters are suitable for use in battery chargers that are designed to operate with extremely low output power levels while maintaining a high degree of efficiency. In a manner analogous to this, the focus of the study is not only on ZVT, but also on the zero current switching action of the switches. These switches were created with the auxiliary resonant cells [7] for the applications involving battery storage, as well as with a high voltage gain zero voltage switching isolated DC-DC converter [8]. In addition, the softswitching was accomplished with the help of leakage inductance and an extra snubber capacitor with the IGBTs that were in charge of the primary power supply. In the framework of the applications of energy storage systems in electric cars, this chapter introduces a novel ZVT bidirectional DC-DC converter as a viable solution. The backdrop for these applications is outlined in the previous sentence. The suggested converter is capable of operating in either a boost or buck mode depending on the situation. This chapter proposes using a novel kind of converter that is not isolated from the rest of the circuit in order to bring about the desired transition of zero voltage to the primary switches. This converter would make use of resonant components and operate in concert with active auxiliary devices. The key advantages that this converter may provide are an increased level of efficiency as well as a reduction in the amount of turn-on losses.

### 2. Description of Proposed Bidirectional DC-DC Converter

A schematic representation of the suggested bidirectional DC-DC converter may be seen in Fig. 1. The primary converter switches are denoted by the symbols S1 and S2, and each of these switches is capable of independently transferring output power while operating in either the boost or buck mode.

A modest number of intervals before to the application of the main switch gating signals, the auxiliary circuit switches S1 and S2 are activated in order to accomplish the transition from zero voltage to full voltage in the main switches Sb and Sa. Before applying the gating signal to the main switch, the auxiliary inductors L1 and L2 and the capacitors C1 and Cy are resonating so that the auxiliary switching devices S1 and S2 may receive the signal and then pass it on to the main switch. The operating concept was explained with the use of representations of current flow that were shown in Fig.3 for the boost mode, and Fig.4 illustrated the schematics for the buck mode. Reduced power consumption during the turn-on process of the primary active devices, as well as reduced power consumption during the switching process of the secondary active devices.

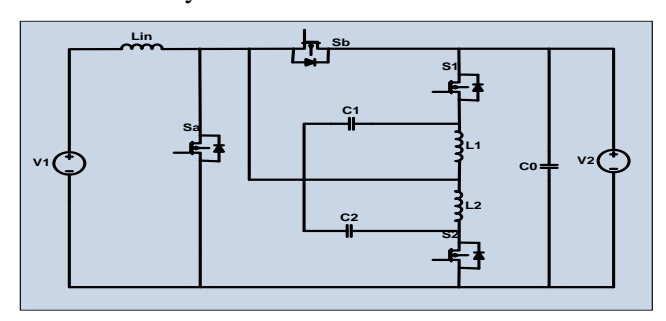


Figure 1: Proposed new ZVT bidirectional DC-DC converter

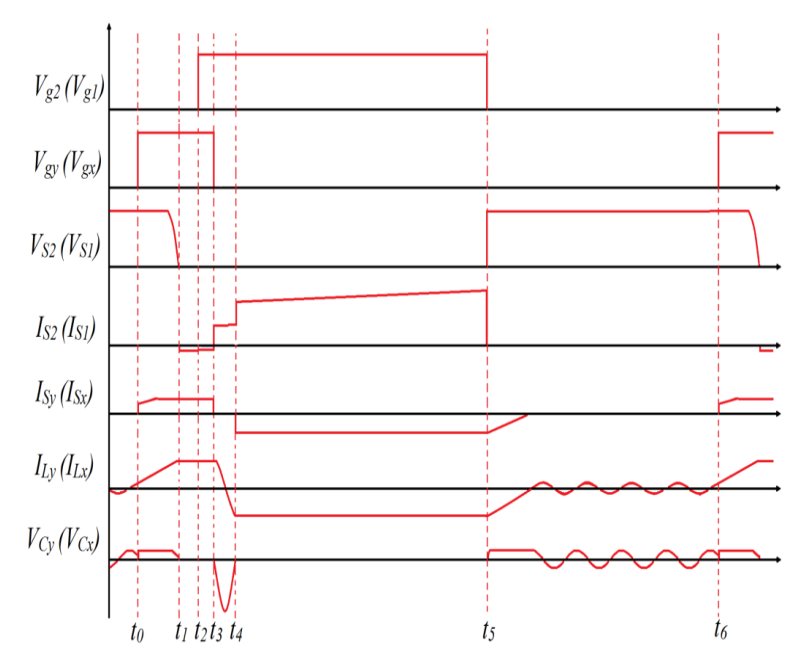


Figure 2: Key waveforms: Boost (Buck) modes

## 3. Principle Of Operation and its Analysis

#### 3.1. Boost mode operation

Figure 2 depicts the usual voltage and current waveforms for the length of one switching cycle (from t0 to t6) and demonstrates how the corresponding current flow models of the boost mode are depicted in the figure. This converter may function in a total of six different topological modes, which are shown from Figure 3 to 6, and are broken down into the following categories.

Mode 1: IGBT S2 is switched on at time t0 in order to ensure zero voltage turn-on for IGBT Sa, which takes place later. The voltage between the collector and the emitter drops in a sinusoidal pattern as it approaches zero; this can be seen quite clearly in Fig. 3 as the main waveforms. At the conclusion of this time period t1, the voltage has dipped to zero, and current in the opposite direction is flowing via the anti-parallel diode of the IGBT Sa. The following equation may be used to represent the current and voltage of an inductor with the symbol L2 and a capacitor with the symbol C2:

$$i_{L2}(t) = I_{in}(t) + \frac{V_0}{Z} \sin \omega (t - t_1)$$

$$V_{C2}(t) = V_0 \cos \omega (t - t_1)$$

$$(2)$$

$$\omega = \frac{1}{\sqrt{L_2 C_2}}$$

$$Z = \sqrt{\frac{L_2}{C_2}}$$

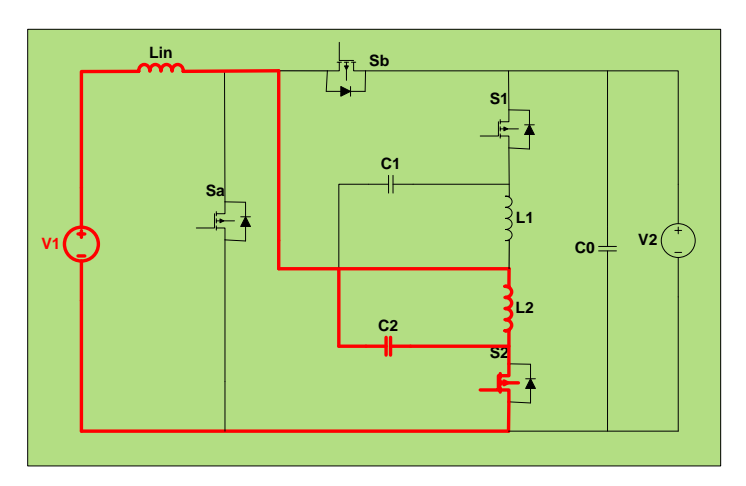


Figure 3: Current flow equivalent circuit for time interval (t0-t1) - boost mode

Mode 2:During the time between t1 and t2, the auxiliary IGBT S2 and the diode of Sa are conducting. The diode of Sa provides the current flow channel for the resonant current that is created by L2 and C2 when the freewheeling mode is active as shown in figure 4. Current and voltage expressions for an inductor with the symbol L2 and a capacitor with the symbol C2 are defined as follows::

$$i_{L2}(t_2) = I_{\min} \frac{V_1}{I} (t - t_2)$$
 (3)

$$V_{C2}(t_2) = 0 (4)$$

Mode 3:Since the diodes of the IGBT Sa and S2 have been conducting during the preceding time intervals, the gate pulses are applied to Sa at the moment t2 when the timing sequence begins. During this phase of freewheeling, the diode of Sa provides the channel for resonant current to follow as shown in figure 4. Current and voltage expressions for an inductor with the symbol L2 and a capacitor with the symbol Cy are defined as follows:

$$i_{L2}(t) = I_{L2}(t_3) + \frac{V_0}{Z}\cos\omega(t - t_4)$$
 (5)

$$V_{C2}(t_3) = -Zi_{L2}(t_3)\sin\omega(t)$$
 (6)

$$V_{C2}(t_4) = 0 (7)$$

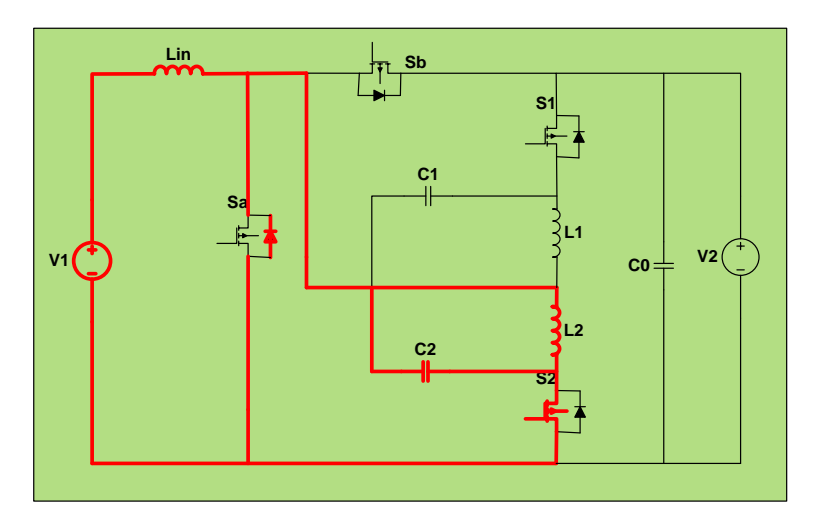


Figure 4: Current flow equivalent circuit for time interval (t1-t2) and for time interval (t2-t3)
- boost mode

Mode 4: From time point t3 until time point t4, the current that flows through the main switch Sa is equal to the output current, while the current that flows through the auxiliary switch is zero as shown in figure 5. The following is the definition of the expression for the inductor L2 current:

$$i_{L2}(t) = I_{in} + \frac{V_1}{L}(t - t_4)$$
 (8)

$$i_{L2}(t) = i_{L2}(t_4) \tag{9}$$

Mode 5: From the t4 to t5 period, there is a current flow in the opposite direction via the auxiliary switch diode, while the current is flowing normally through the main switch. While in this accumulating mode, the input inductor Lin is allowed to build up its total value as shown in figure 5.

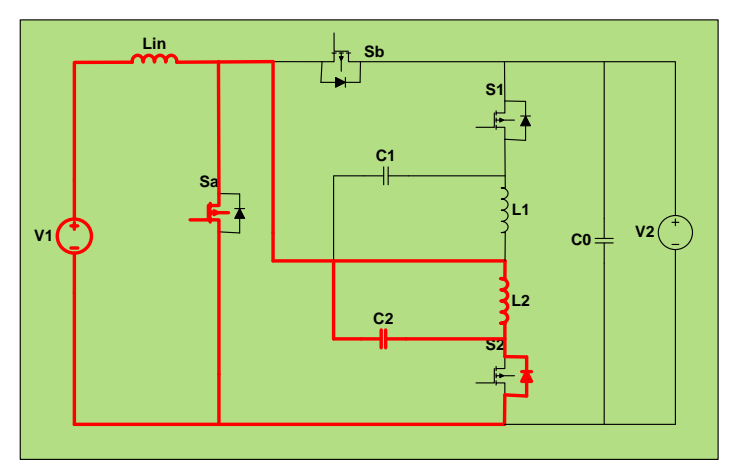


Figure 5: Current flow equivalent circuit for time interval (t3-t4) and for time interval (t4-t5) *Nanotechnology Perceptions* Vol. 20 No.5 (2024)

#### - boost mode

Mode 6: Because there is output current flow by the energised input inductor Lin during the period t5-t6, all of the switching devices are switched off at this time. Throughout the duration of this powering mode, the output power is transferred via Sb's L-body diode as shown in figure 6.

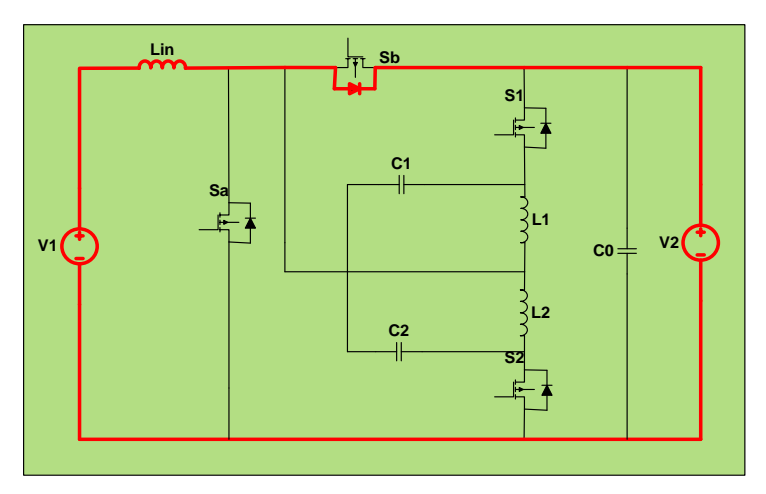


Figure 6: Current flow equivalent circuit for time interval (t5-t6) - boost mode

# 3.2 Buck mode operation

As seen in Figure 2, the buck mode functioning may be broken down into six distinct topological modes. These modes are determined by the normal voltage and current waveforms. Figure 7 to 10provides visual representations of the corresponding operating models. Whenever this mode is active, the Sb is functioning as the power transfer switch, and the S1 has the capability of functioning as an auxiliary switch. However, in order to prevent the main IGBT from being gated, the auxiliary switch can only be used for a very little period of time before it becomes inoperable. The following is a description of each of the six distinct topological modes:

Mode 1: The supplementary IGBT S1 is switched on at time t0 in order to ensure gentle turnon for the IGBT Sb, which occurs later. The auxiliary inductor L1 and the auxiliary inductor C1 are resonating with one another as shown in figure 7. During this resonant phase, the voltage of the switch gradually goes from one value to the next until it reaches zero at time t1.

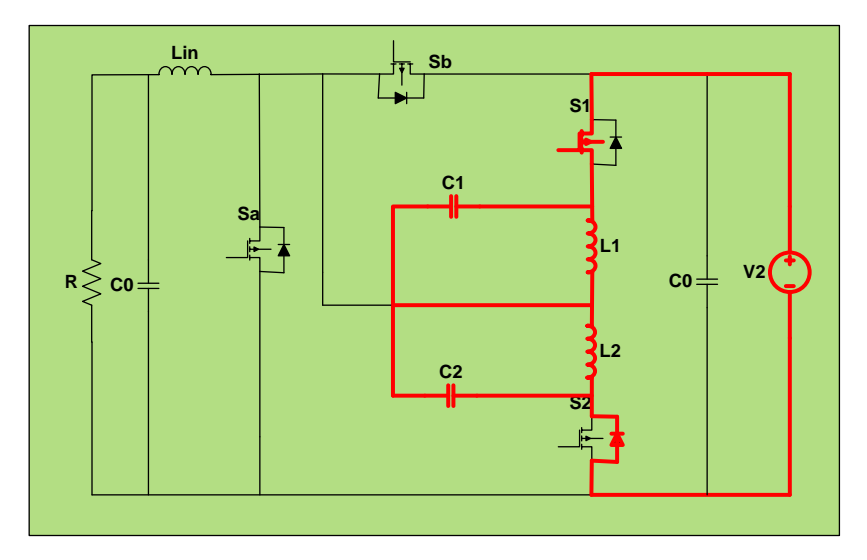


Figure 7: Current flow equivalent circuit for time interval (t0-t1) - buck mode

Mode 2:During this freewheeling mode, at the time t1, the diode of Sb begins conducting in order to create a free wheeling channel in order to enable resonant tank current, which is provided by L1,C1 as shown in figure 8. The level of the output current is reached by the current via the resonant inductor, L1.

Mode 3:Beginning at time t2, the diode of switch S2 continues to conduct, while gating signals are also being applied to switch S1 at the same time. When this time period t2 has passed, the diode of Sa will have been switched off, but the output current level will have been maintained by the inductor current as shown in figure 8.

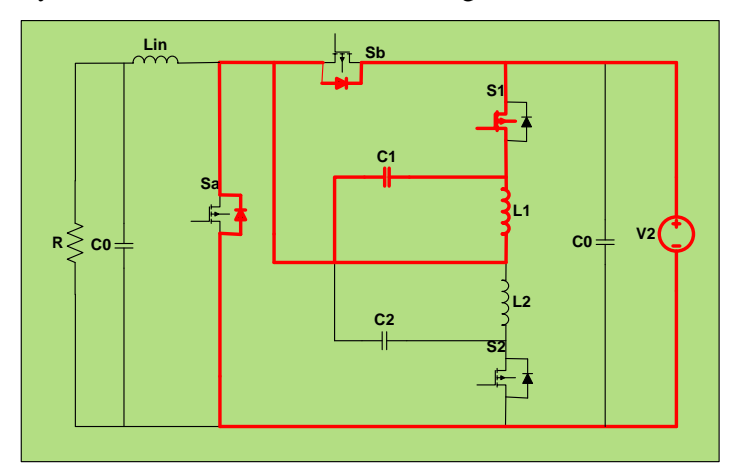


Figure 8: Current flow equivalent circuit for time interval (t1-t2) and for time interval (t2-t3) - buck mode

Mode 4: At time t3, the auxiliary IGBT S1 is shut off, which results in the current flowing through it being zero. The primary IGBT Sb begins conducting, and an output power flow may be seen through the Sb-Lin connection as shown in figure 9. During this mode of

powering, the current flowing through the inductor L1 linearly falls until it reaches zero, and the resonant capacitor C1 is charged to the level of the input voltage before being discharged at t4.

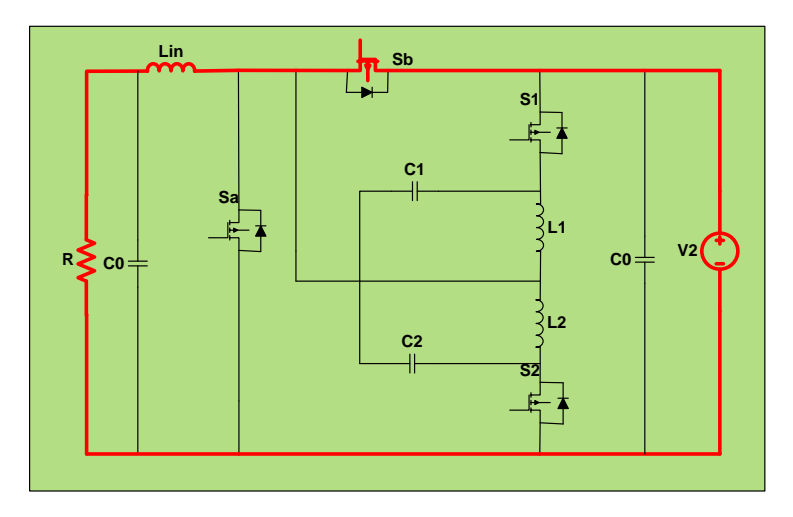


Figure 9: Current flow equivalent circuit for time interval (t3-t4) - buck mode

Mode 5: During this powering mode, the IGBT Sb is conducting from t4 to t5, and the diode of S1 offers a freewheeling channel for the resonant tank current. Throughout the whole of this time, the output power is transferred to the resistance R by way of the V2-Sb-Lin circuit. At time t5, both the diode of S1 and the IGBT Sb are switched off as shown in figure 10.

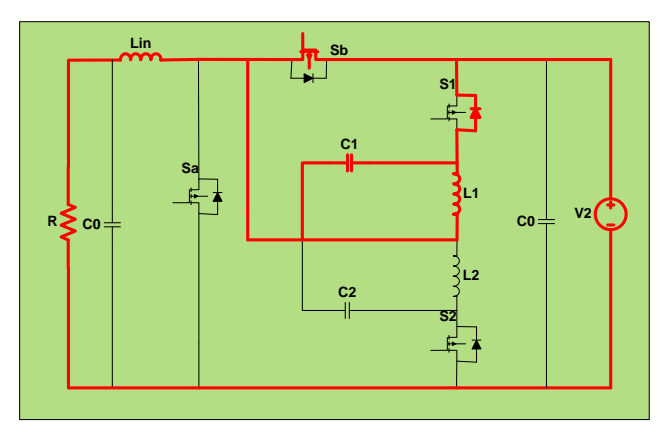


Figure 10: Current flow equivalent circuit for time interval (t4-t5) - buck mode

Mode 6: From t5-t6, all the switches are turned-off. Therefore, there is no power to be delivered to the load.

# 4. Design Analysis

The auxiliary resonant elements Ly, Cy are defined as a function of the current stress on the auxiliary IGBT, given by Y1 which is directly related to conduction losses, it is chosen less

than the value 1.244 in this converter.

$$Y_{1} = \left[ 1 + \left( \frac{V_{0}}{ZI_{in}} \right) \right] \tag{10}$$

The total soft-commutation (ZVT) time is given by tZVT

$$t_{ZVT} = \frac{I_{in}L_2}{V_1} + \frac{\pi\sqrt{L_2C_2}}{2}$$
 (11)

By solving the (9) and (10) for Ly and Cy, the following expressions can be found

$$L_2 \le \frac{V_0 t_{ZVT}}{I_0 (1 + \frac{\pi (Y_1 - 1)}{2})} \tag{12}$$

$$C_2 \le \frac{L_2(1 + \frac{V_1}{Z})^2}{V_1^2} \tag{13}$$

Table 1: Parameters considered for the proposed converter

Parameter	Type	Value
Resonant Capacitors		4nF
Resonant Inductors		25μΗ
Input inductor		250μΗ
Input voltage	Boost mode	100V
Input voltage	Buck mode	200V
Output Capacitor		470μF
Switching frequency		50kHz
Duty ratio		0.5-0.6

In Table 1, the input and output parameters of the converter are presented for your perusal. The value of Y1 determines which numerical solution to use for the expressions (10) and (11), respectively. The value of Y1 is determined to be 1.244, and the time period soft-transition (ZVT) is set to 10%; the values of resonant inductors L1,L2 are obtained as 5 H based on equation (12), and the values of resonant capacitors C1,C2 may be chosen to be 10 nF based on equation (13). The characteristic impedance (Z) of this resonant tank was calculated to be 81.64 after taking into account the values of the resonant parts. Because the characteristic impedance of the resonant tank has the potential to influence the voltage and current strains that are placed on the switches, its value should be lower than 81.64 ohms. The soft transition (ZVT) time interval may be determined by using equation (11), and it is around 2.8 microseconds long. This represents approximately 10% of the total switching period, which refers to when the switch is turned on and off.

The suggested converter was created by making use of MATLAB simulink, and it was accompanied on 100V as an input while operating in boost mode and 200V when operating in buck mode. This converter has been put through its paces with a switching frequency of 50 kHz while producing 1.5 kW of output power.

#### 5. Results and Discussions

The suggested converter was created by making use of MATLAB simulink, and it was accompanied on 100V as an input while operating in boost mode and 200V when operating in buck mode. This converter has been put through its paces with a switching frequency of 50 kHz while producing 1.5 kW of output power.

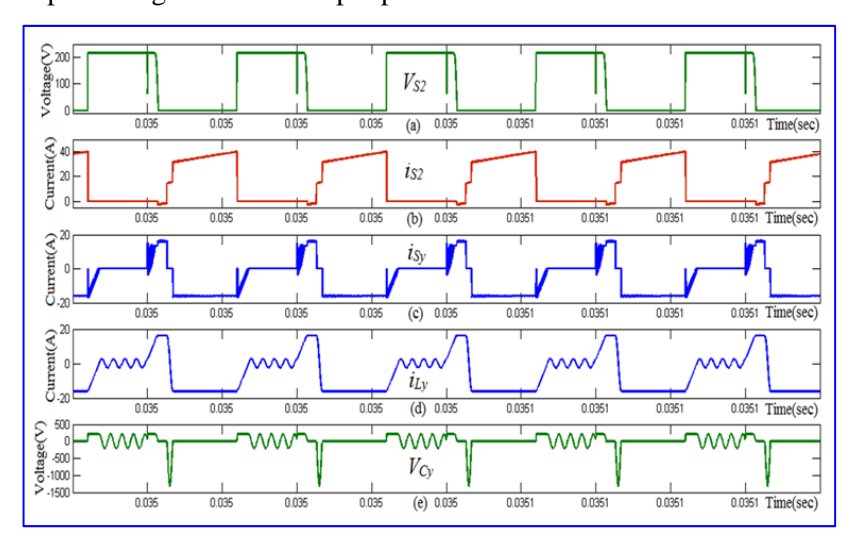


Figure 5: Simulated Results. (a) & (b) Voltage and currents of S2 (c) Current of S2(d) Auxiliary resonant inductor current (L2) (e) Auxiliary resonant capacitor (C2) voltage: Boost mode

The voltage and currents of the Sa are shown in Fig.5 (a) and (b), respectively, while the currents of S2 and L2 are displayed in Fig.5 (c) and (d), respectively, and the voltage of the capacitor C2 in boost mode is displayed in Fig.5 (e).

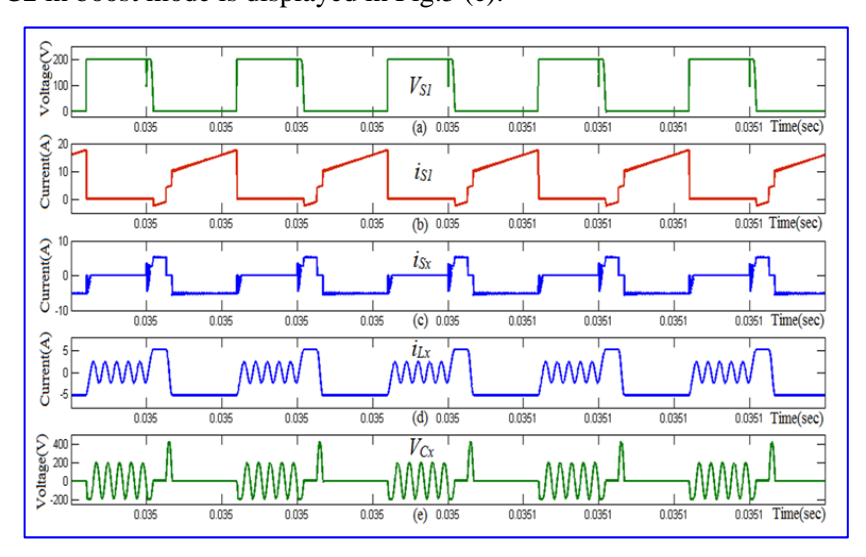


Figure 6: Simulated Results (a) Voltage of Sb (b) Current of Sb (c) Current of the S1(d)

Auxiliary Resonant Inductor Current (L1) (e) Auxiliary Resonant Capacitor (C1) voltage: Buck mode

The voltage and currents of the Sb are shown in Fig.6 (a) and (b), respectively. The currents of the S1 and L1 are shown in Fig.6 (c) and (d), respectively, and Fig.6 (e) displays the voltage of the capacitor C1 in buck mode. The findings that were obtained demonstrated that the predicted theoretical assumptions were correct.

#### 6. Conclusions

In this research work, a novel ZVT non-isolated bidirectional DC-DC converter is proposed, the operating principles are detailed, and experimental results are also shown. The traditional converter was enhanced by the addition of auxiliary components, which enabled the achievement of the zero-voltage transition to the main switch. The effectiveness achieved was very close to 95% in each mode. The converter that has been presented is appropriate for use in battery storage applications in hybrid electric cars and DC traction vehicles because it has decreased turn-on stresses, decreased switching power losses, and better efficiency.

#### References

- M. Sigala, A. Beer, L. Hodgson, and A. O'Connor, Big Data for Measuring the Impact of Tourism Economic Development Programmes: A Process and Quality Criteria Framework for Using Big Data. 2019.
- 2. G. Nguyen et al., "Machine Learning and Deep Learning frameworks and libraries for large-scale data mining: a survey," Artif. Intell. Rev., vol. 52, no. 1, pp. 77–124, 2019, doi: 10.1007/s10462-018-09679-z.
- 3. C. Shorten and T. M. Khoshgoftaar, "A survey on Image Data Augmentation for Deep Learning," J. Big Data, vol. 6, no. 1, 2019, doi: 10.1186/s40537-019-0197-0.
- 4. R. Vinayakumar, M. Alazab, K. P. Soman, P. Poornachandran, A. Al-Nemrat, and S. Venkatraman, "Deep Learning Approach for Intelligent Intrusion Detection System," IEEE Access, vol. 7, pp. 41525–41550, 2019, doi: 10.1109/ACCESS.2019.2895334.
- 5. K. Sivaraman, R. M. V. Krishnan, B. Sundarraj, and S. Sri Gowthem, "Network failure detection and diagnosis by analyzing syslog and SNS data: Applying big data analysis to network operations," Int. J. Innov. Technol. Explor. Eng., vol. 8, no. 9 Special Issue 3, pp. 883–887, 2019, doi: 10.35940/ijitee.I3187.0789S319.
- 6. A. D. Dwivedi, G. Srivastava, S. Dhar, and R. Singh, "A decentralized privacy-preserving healthcare blockchain for IoT," Sensors (Switzerland), vol. 19, no. 2, pp. 1–17, 2019, doi: 10.3390/s19020326.
- 7. Vijay Muni, T., Lalitha, S. V. N. L., Rajasekhar Reddy, B., Shiva Prasad, T., & Sai Mahesh, K. (2017). Power management system in PV systems with dual battery. International Journal of Applied Engineering Research, 12(Special Issue 1), 523–529.
- 8. Prasanna Kumar Inampudi, Dr Chandrasekar Perumal, Venkata Ramana Guntreddi, & Tadanki Vijay Muni. (2024). A Novel DC-DC Boost Converter with Coupled Inductors for High Gain and Smooth Switching . Journal of Advanced Research in Applied Sciences and Engineering Technology, 48(2), 92–104. https://doi.org/10.37934/araset.48.2.92104
- 9. F. Al-Turjman, H. Zahmatkesh, and L. Mostarda, "Quantifying uncertainty in internet of medical things and big-data services using intelligence and deep learning," IEEE Access, vol. 7, pp. 115749–115759, 2019, doi: 10.1109/ACCESS.2019.2931637.
- 10. S. Kumar and M. Singh, "Big data analytics for healthcare industry: Impact, applications, and *Nanotechnology Perceptions* Vol. 20 No.5 (2024)

- tools," Big Data Min. Anal., vol. 2, no. 1, pp. 48–57, 2019, doi: 10.26599/BDMA.2018.9020031.
- 11. Sathish, T., Ağbulut, Ü., Kumari, V., Rathinasabapathi, G., Karthikumar, K., Rama Jyothi, N., ... Saravanan, R. (2023). Energy recovery from waste animal fats and detailed testing on combustion, performance, and emission analysis of IC engine fueled with their blends enriched with metal oxide nanoparticles. Energy, 284. https://doi.org/10.1016/j.energy.2023.129287
- 12. L. M. Ang, K. P. Seng, G. K. Ijemaru, and A. M. Zungeru, "Deployment of IoV for Smart Cities: Applications, Architecture, and Challenges," IEEE Access, vol. 7, pp. 6473–6492, 2019, doi: 10.1109/ACCESS.2018.2887076.
- Ramana, G. V., Muni, T. V., Subbarayudu, C. B. V., Parimala, V., Suneela, B., & Raj, E. F. I. (2022). Improving the Maximum Power Point Tracking in Wind Farms with PID and Artificial Intelligence Controllers for Switched Reluctance Generators. In 2022 International Conference on Futuristic Technologies, INCOFT 2022. Institute of Electrical and Electronics Engineers Inc. https://doi.org/10.1109/INCOFT55651.2022.10094347
- 14. B. P. L. Lau et al., "A survey of data fusion in smart city applications," Inf. Fusion, vol. 52, no. January, pp. 357–374, 2019, doi: 10.1016/j.inffus.2019.05.004.
- 15. Kishore, D. R., Muni, T. V., Raja, B. S., Pushkarna, M., Goud, B. S., AboRas, K. M., & Alphonse, S. (2023). Grid-Connected Solar PV System with Maximum Power Point Tracking and Battery Energy Storage Integrated with Sophisticated Three-Level NPC Inverter. International Transactions on Electrical Energy Systems, 2023. https://doi.org/10.1155/2023/3209485
- Pradeep, K., Kumar, K. V., Muni, T. V., Rayudu, K., Prakash, A., & Kumar, P. R. (2023). Single-Phase Grid-Connected Photovoltaic Systems using an ANFIS MPPT Algorithm with Grey-Wolf Optimisation. In 2023 IEEE 3rd International Conference on Smart Technologies for Power, Energy and Control, STPEC 2023. Institute of Electrical and Electronics Engineers Inc. https://doi.org/10.1109/STPEC59253.2023.10430654
- 17. Prakash, R. B. R., Srinivasa Varma, P., Ravikumar, C., Vijay Muni, T., Srinivasulu, A., Bagadi, K., ... Sathish, K. (2023). Intelligent Energy Management for Distributed Power Plants and Battery Storage. International Transactions on Electrical Energy Systems, 2023. https://doi.org/10.1155/2023/6490026
- 18. Y. Wu et al., "Large scale incremental learning," Proc. IEEE Comput. Soc. Conf. Comput. Vis. Pattern Recognit., vol. 2019-June, pp. 374–382, 2019, doi: 10.1109/CVPR.2019.00046.
- Jayaraman, R., Tummapudi, S., Prakash, R. B. R., & Vijay Muni, T. (2023). Analysis of sliding mode controller based DSTATCOM for power quality improvement in distribution power system. Materials Today: Proceedings, 80, 3675–3681. https://doi.org/10.1016/j.matpr.2021.07.360
- 20. Baig, K., Prudhvi Raj, K., Raja Sekhar, G. G., Vijay Muni, T., & Kiran Kumar, M. (2020). Power quality enchancement with active power control. Journal of Critical Reviews, 7(9), 739–741. https://doi.org/10.31838/jcr.07.09.143
- 21. A. Mosavi, S. Shamshirband, E. Salwana, K. wing Chau, and J. H. M. Tah, "Prediction of multi-inputs bubble column reactor using a novel hybrid model of computational fluid dynamics and machine learning," Eng. Appl. Comput. Fluid Mech., vol. 13, no. 1, pp. 482–492, 2019, doi: 10.1080/19942060.2019.1613448.
- 22. Muni, T. V., & Lalitha, S. V. N. L. (2020). Implementation of control strategies for optimum utilization of solar photovoltaic systems with energy storage systems. International Journal of Renewable Energy Research, 10(2), 716–726. https://doi.org/10.20508/ijrer.v10i2.10565.g7943
- 23. V. Palanisamy and R. Thirunavukarasu, "Implications of big data analytics in developing healthcare frameworks A review," J. King Saud Univ. Comput. Inf. Sci., vol. 31, no. 4, pp. 415–425, 2019, doi: 10.1016/j.jksuci.2017.12.007.

- 24. J. Sadowski, "When data is capital: Datafication, accumulation, and extraction," Big Data Soc., vol. 6, no. 1, pp. 1–12, 2019, doi: 10.1177/2053951718820549.
- 25. J. R. Saura, B. R. Herraez, and A. Reyes-Menendez, "Comparing a traditional approach for financial brand communication analysis with a big data analytics technique," IEEE Access, vol. 7, pp. 37100–37108, 2019, doi: 10.1109/ACCESS.2019.2905301.
- 26. D. Nallaperuma et al., "Online Incremental Machine Learning Platform for Big Data-Driven Smart Traffic Management," IEEE Trans. Intell. Transp. Syst., vol. 20, no. 12, pp. 4679–4690, 2019, doi: 10.1109/TITS.2019.2924883.
- 27. S. Schulz, M. Becker, M. R. Groseclose, S. Schadt, and C. Hopf, "Advanced MALDI mass spectrometry imaging in pharmaceutical research and drug development," Curr. Opin. Biotechnol., vol. 55, pp. 51–59, 2019, doi: 10.1016/j.copbio.2018.08.003.
- 28. C. Shang and F. You, "Data Analytics and Machine Learning for Smart Process Manufacturing: Recent Advances and Perspectives in the Big Data Era," Engineering, vol. 5, no. 6, pp. 1010–1016, 2019, doi: 10.1016/j.eng.2019.01.019.
- 29. Y. Yu, M. Li, L. Liu, Y. Li, and J. Wang, "Clinical big data and deep learning: Applications, challenges, and future outlooks," Big Data Min. Anal., vol. 2, no. 4, pp. 288–305, 2019, doi: 10.26599/BDMA.2019.9020007.
- 30. M. Huang, W. Liu, T. Wang, H. Song, X. Li, and A. Liu, "A queuing delay utilization scheme for on-path service aggregation in services-oriented computing networks," IEEE Access, vol. 7, pp. 23816–23833, 2019, doi: 10.1109/ACCESS.2019.2899402.
- 31. G. Xu, Y. Shi, X. Sun, and W. Shen, "Internet of things in marine environment monitoring: A review," Sensors (Switzerland), vol. 19, no. 7, pp. 1–21, 2019, doi: 10.3390/s19071711.
- 32. M. Aqib, R. Mehmood, A. Alzahrani, I. Katib, A. Albeshri, and S. M. Altowaijri, Smarter traffic prediction using big data, in-memory computing, deep learning and gpus, vol. 19, no. 9. 2019.
- 33. S. Leonelli and N. Tempini, Data Journeys in the Sciences. 2020.N. Stylos and J. Zwiegelaar, Big Data as a Game Changer: How Does It Shape Business Intelligence Within a Tourism and Hospitality Industry Context? 2019.
- 34. Q. Song, H. Ge, J. Caverlee, and X. Hu, "Tensor completion algorithms in big data analytics," arXiv, vol. 13, no. 1, 2017.